
Article:
Wilson, Sarah orcid.org/0000-0001-5914-5085, Lolley, James, Solis Meza, Eduardo et al. (4 more authors) (2024) Extreme ultraviolet laser ablation and time of flight mass spectrometry of gold, aluminum, and copper targets. Physics of Plasmas. ISSN: 1089-7674

https://doi.org/10.1063/5.0212133

RESEARCH ARTICLE | AUGUST 01 2024

Extreme ultraviolet laser ablation and time-of-flight mass spectrometry of gold, aluminum, and copper targets

S. A. Wilson ; L. A. Rush ; E. Solis Meza ; J. A. Lolley ; J. J. Rocca; C. S. Menoni ; G. J. Tallents

Phys. Plasmas 31, 082702 (2024)
https://doi.org/10.1063/5.0212133

Extreme ultraviolet laser ablation and time-of-flight mass spectrometry of gold, aluminum, and copper targets

Cite as: Phys. Plasmas **31**, 082702 (2024); doi: 10.1063/5.0212133
Submitted: 8 April 2024 · Accepted: 8 July 2024 ·
Published Online: 1 August 2024

S. A. Wilson,[1,a] L. A. Rush,[2] E. Solis Meza,[2] J. A. Lolley,[3] J. J. Rocca,[2] C. S. Menoni,[2] and G. J. Tallents[3]

AFFILIATIONS

[1]Department of Chemistry, The University of York, York YO10 5DD, United Kingdom
[2]Electrical and Computer Engineering Department, Colorado State University, Fort Collins, Colorado 80523, USA
[3]York Plasma Institute, School of Physics, Engineering and Technology, The University of York, York YO10 5DD, United Kingdom

[a]Author to whom correspondence should be addressed: sarah.wilson3@york.ac.uk

ABSTRACT

An ablation crater depth estimation model, founded on the concept of an ionizing bleaching wave, has been developed for metal targets irradiated by an extreme ultraviolet (EUV) laser. Two EUV capillary discharge lasers operating at a wavelength of 46.9 nm were focused onto targets of gold, aluminum, and copper using two different experimental setups to maximize the laser fluence range. The experimental ablation craters were measured using an atomic force microscope, and the depths were compared to the ionizing wave model. The model depends on the dominant ion charge of the ablated plasma, which was measured experimentally using the low fluence setup with a time-of-flight mass spectrometer. The measured ablation depths and ion charges at low fluences are in agreement with the model. The ablation crater depths in the higher fluence range confirmed the trends predicted by the model, showing potential to expand its use to other materials and fluence ranges.

The development of varied extreme ultraviolet (EUV) sources, such as free-electron lasers and capillary discharge lasers,[1] has led to applications in lithography,[2] nano-machining,[3] and the production of warm dense plasmas.[4] EUV radiation operating at a wavelength of 13.5 nm is particularly vital to the production of semiconductor devices.[5] EUV sources have been incorporated into mass spectrometers for material characterization at the nanoscale by taking advantage of the EUV laser's high absorptivity and efficient photoionization.[6–8]

EUV lasers interact with materials via direct photo-ionization, which produces cooler, denser plasmas than optical/IR/UV laser interactions. The strongly coupled warm dense plasmas are important in inertial confinement fusion experiments. As the fuel pellet is compressed, the material will pass through plasma densities and temperatures in the warm dense plasma regime. Many astrophysical plasmas also exhibit the physics of warm dense plasmas, particularly in cool dense stars and planetary cores.

Additionally, EUV lasers offer a route toward sub-micrometer ablation that is not possible with optical lasers. The short wavelength of EUV lasers allows for a reduction in the diffraction limit, resulting in a reduction in the achievable focal spot diameter. The shorter wavelength also means an increase in critical density, enabling the laser to penetrate further into a solid density material.

With the increase in applications for EUV sources, a deeper understanding of EUV interactions with solid materials is needed. Previous work has investigated the plasma properties of EUV and optical wavelength interactions with metal and plastic targets.[9–11] Here, we investigate the trends in ablated crater depths and the resulting time-of-flight (TOF) mass spectra in metals over a range of laser fluences using an EUV capillary discharge laser that operates at a wavelength of 46.9 nm.[12] The experimental results are used to establish a model for estimating the ablation depth for metal targets based on the characteristics of the material and the ionization of the resulting plasma.

The model predicts the ablation crater depth in solid targets when irradiated with an EUV capillary discharge laser, according to the level of ionization of the plasma produced at 46.9 nm. This is achieved using two experimental setups shown in Figs. 1 and 2. The ion charge to mass ratio is measured at low fluence experimentally by

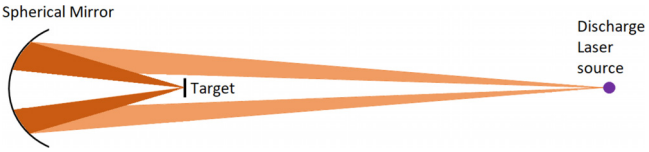

FIG. 1. A schematic of the EUV discharge laser for high fluence ablation. A spherical multi-layer mirror reflects the laser output onto a solid target. Fluences on target with this arrangement ranged from 20 up to 120 J/cm^2.

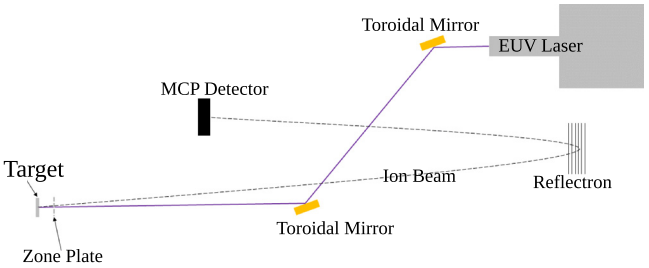

FIG. 2. A schematic of the EUV TOF setup used for low fluence ablation and ionization measurements. Two gold-coated toroidal mirrors are used to guide and collimate the beam to illuminate the zone plate that focuses the laser onto the target. The ions produced in the laser-created plasma are accelerated into the TOF region and subsequently detected by a microchannel plate (MCP). Fluences on target with this arrangement ranged from 0.1 up to 6 J/cm^2.

TOF mass spectrometry, and the ablation crater depth is measured post-shot using an atomic force microscope for all fluence ranges.

In the interaction of focused EUV laser pulses with solid targets, the laser pulse is absorbed at the target, photoionizing atoms and molecules. This is because the critical electron density in the EUV laser-created plasma is an order of magnitude larger than when ablating with optical lasers.[13]

The critical density, n_{crit}, is defined as follows:

$$n_{crit} = \frac{\varepsilon_0 m \omega^2}{e^2} \tag{1}$$

$$\approx \frac{1.11 \times 10^{21}}{\lambda^2(\mu\text{m})}\ \text{cm}^{-3}, \tag{2}$$

where λ is the wavelength in micrometers. An optical laser with a wavelength of 1 μm has a critical density of 1.1×10^{21} cm^{-3}, whereas an EUV laser operating at 46.9 nm has a critical density of 5×10^{23} cm^{-3}. The higher critical density significantly modifies the laser interactions with solid targets because a solid material of ionization level Z, atomic mass M, and density ρ (g cm^{-3}) with proton mass m_H, has a free electron number density, n_{solid}, which is given by the following equation:

$$n_{solid} = \frac{Z\,\rho}{M\,m_H} = \frac{Z}{M}\,\frac{\rho}{1.67}\ 10^{24}\ \text{cm}^{-3}. \tag{3}$$

Equation (3) shows that a solid target with a low ionization level will produce densities much higher than the critical density of an optical laser. Optical lasers cannot penetrate through a solid-density plasma due to the low critical density. The higher critical density of the EUV radiation allows the laser pulse to penetrate through an ablated plasma plume of near-solid density and continue interacting with the target material throughout the duration of the pulse, thus changing the way in which the radiation interacts with the target.

A study by Tallents *et al.*[14] modeled x rays with photon energies of 750 eV generated by free-electron lasers and 89 eV photons generated by a laboratory-based EUV laser ablating iron and carbon targets. This study assumes that the x-ray and EUV radiation interact with the target as an ionizing wave. An ionizing wave is assumed when the incident photon energy is near or slightly above an absorption edge. The EUV radiation quickly ionizes the target so the absorption edge of the material is shifted to a higher energy, and the target becomes transparent or bleached. The energy density required for ionization to occur, E_{bleach}, can be calculated from the energy required to remove sufficient electrons so that the ionization energy shifts above the photon energy. It is assumed that a small thickness, Δx, of the target is ablated in a time, Δt (i.e., the laser pulse duration), by the focused laser intensity, I, so that

$$I\Delta t = E_{bleach}\Delta x. \tag{4}$$

Rearranging Eq. (4) gives the velocity, v_{bleach}, of the ionizing wave through the target

$$v_{bleach} = \frac{\Delta x}{\Delta t} = \frac{I}{E_{bleach}}. \tag{5}$$

By integrating the intensity of the ablation with respect to time, the fluence, $F = \int I dt$, and crater depth, $D = \int v_{bleach} dt$, are calculated as

$$D = \frac{\int I dt}{E_{bleach}} = \frac{F}{E_{bleach}}. \tag{6}$$

The value for E_{bleach} is given by

$$E_{bleach} = H_{ablation} + E_t + E_{ion}, \tag{7}$$

where $H_{ablation}$ is the latent heat of ablation, E_t is the thermal energy of the ions, and E_{ion} is the energy required to ionize ablated material to a determined degree of ionization. The thermal energy of the ions, E_t, is given by

$$E_t = \frac{3}{2}\frac{(Z_i + 1)\rho}{A m_p} k_B T, \tag{8}$$

where Z_i is the ion charge, ρ is the mass density, A is the atomic mass, and m_p is the mass of a proton. The temperature T for the evaluation of E_t and $H_{ablation}$ is assumed to be equal to the peak temperature associated with a determined ionization.

The ionization energy, E_{ion}, is given by

$$E_{ion} = \left(\frac{\rho}{A\,m_p}\right)\sum E_d, \tag{9}$$

where E_d is the ionization energy in eV for each degree of ionization. The depth of ablation is then given by

$$D = \frac{F}{H_{ablation} + E_t + \left(\frac{\rho}{A\,m_p}\right)\sum E_d}. \tag{10}$$

In this study, the ionizing wave model is used to estimate ablation crater depths for targets of gold, aluminum, and copper using an EUV laser operating at a wavelength of 46.9 nm, which is then compared to experimental data. For low fluence laser interactions, the appropriate ion charge achieved in the ablation process is measured using TOF mass spectrometry of the expanding plasma plume. The ablation plasma typically has a range of ion charges, the most dominant of these is compared to the ionizing wave model. Results have shown that when compared to ablation crater depths at high fluence, the model can also be applied. Recombination can decrease the ionization level detected by the mass spectrometer, suggesting that a lower ionization level is suitable for the model, as the recombination energy is converted into expanding motion.

To enable EUV irradiation of solid targets over a wide range of fluences, two different focusing arrangements were employed using (i) large reflective mirrors and an laser system with maximum energy (50 μJ), for high fluence irradiation (10–120 J/cm^2), and (ii) a Fresnel zone plate (outer diameter of 500 μm, numerical aperture of 0.12, and 10% efficiency when operated in the first order[6]) using a laser with maximum energy of 10 μJ, for low fluence irradiation (0.1–6 J/cm^2). The two EUV capillary discharge lasers used in this study, developed at Colorado State University (CSU) by Rocca *et al.*,[12,15] use Neon-like Argon ions (i.e., Ar^{8+}) as the lasing medium, resulting in an operating wavelength of 46.9 nm (26.4 eV photon energy),[16] with pulse duration of 1.2 ns, and rep-rates of 1–10 Hz. Gold, aluminum (Goodfellow, thickness 0.02 mm), and copper (Goodfellow, thickness 0.02 and 500 nm deposited on a silicon substrate) targets were ablated with single EUV laser shots. The resulting crater profiles were measured with an atomic force microscope. Lineouts of the craters are shown in Fig. 3. These targets were chosen as they present a range of different optical properties for metals.

The EUV laser setup, used to ablate targets at high fluences, focuses the EUV beam with a single spherical mirror, coated with either a scandium silicon (Sc/Si) multi-layer (45% reflectivity) or an unprotected gold coating (8% reflectivity), as shown in Fig. 1. The annular profile of the EUV capillary discharge laser[6,15,17] allows for on-axis focusing onto a target positioned in the annulus of the beam without significantly obstructing the beam path. An on-axis spherical mirror minimizes astigmatism and reduces spherical aberrations, producing a near-diffraction limited focal spot with minimal loss of the incoming laser radiation from a target blocking the beam. The EUV discharge laser energy ranges from 16 to 30 μJ. The average energy at the target is 11.5 μJ using the Sc/Si mirror and 2 μJ using the Au-coated mirror.

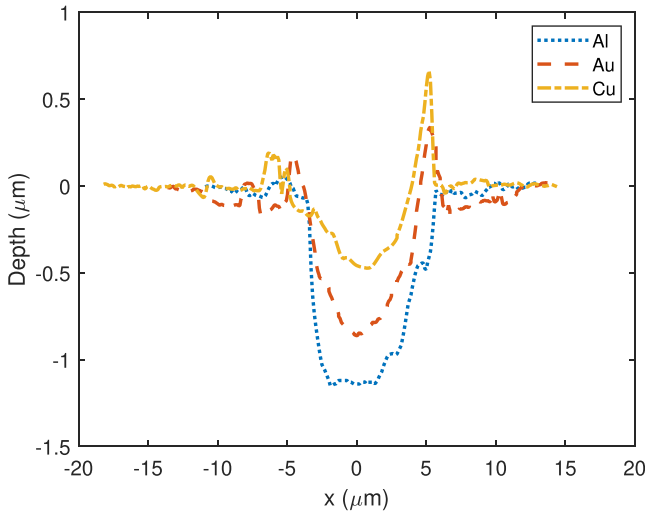

FIG. 3. 1D profiles of ablation craters from single shots on aluminum (blue), gold (red), and copper (purple) focused using a scandium silicon multi-layer mirror with a radius of curvature 100 mm.

The lower fluence data were collected using the EUV capillary discharge laser connected to a time-of-flight mass spectrometer (Fig. 2), also developed at CSU.[6–8] The EUV TOF allows for mass-to-charge ratio analysis of the ablated ions from the sample area. The EUV laser is guided and collimated by two gold-coated toroidal mirrors set at grazing incidence. The EUV laser is focused onto the sample using a Fresnel zone plate (FZP) with 0.12 NA and operated in first order. The FZP has a very high quality focus and gives nanoscale diffraction-limited focal spots.[6–8] A 6 kV potential between the target and the ground grid is used to accelerate the ions into the TOF spectrometer. Ions enter the field-free region of the TOF tube and are deflected by a reflectron to image on a multichannel plate. The reflectron doubles the ion's flight path, resulting in better separation of ion packets.[6]

The EUV laser energy on the EUV TOF setup is measured using an aluminum inline detector.[18] The laser energy is attenuated and controlled with an argon gas cell located immediately after the capillary laser output. The gas cell is isolated from the target vacuum as the laser pulse passes through a small aperture with differential pumping. Control of the laser's energy allows for control of sample ablation. The EUV transmission through the cell shows an exponential dependence as a function of argon pressure.[18] The EUV TOF uses a version of the EUV discharge laser with a maximum pulse energy of 10 μJ.[15] Combined with the optical transmission of 1.5×10^{-3} from the mirror reflectivity and the efficiency of the zone plate, the laser energy reaching the sample ranges from 15 to 4.5 nJ. The fluence for each shot was determined using the measured pulse energy and the measured ablation area, with the approximation that the fluence is constant over the ablated area. Ablation profiles from single laser shots were measured post-shot using an atomic force microscope (AFM), with the target fixed at the FZP's 2.14 mm focal length. Mass spectra were recorded for each laser shot using the low fluence setup (Fig. 2) and used to identify the ion charge of the different metals.[6–8]

Equation (10) can be used to estimate of the depth of ablation craters obtained in Au, Al, and Cu at different fluences based on the corresponding material properties and degree of ionization. Post-ablation analysis using an AFM gives an ablation crater depth and width for the corresponding mass spectrum data. From this, we can calculate the energy density of each laser shot on target. The energy density can be compared to E_{bleach} in order to estimate the level of ionization of the ablated plasma. The energy density of the target material as it is ablated can be estimated using the following equation:

$$U = \frac{E_{laser}}{V_{ab}}, \tag{11}$$

where U is the energy density in J/cm^3, E_{laser} is the laser energy on target in J, and V_{ab} is the volume of ablated material in cm. Figures 4–6

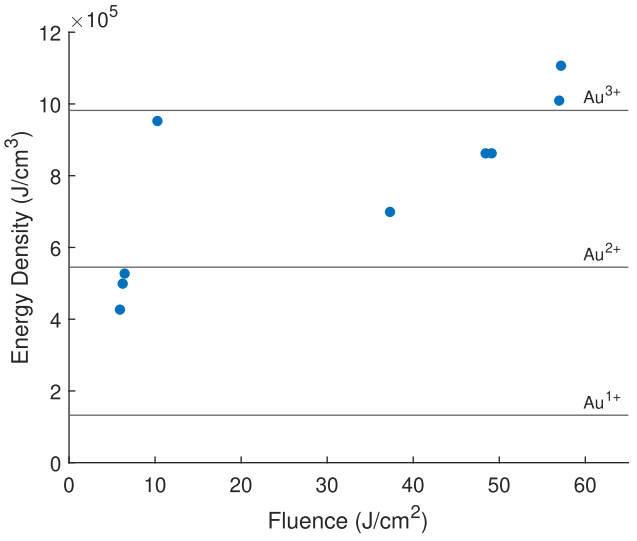

FIG. 4. The plasma energy density determined from the experimental ablation volume as a function of experimental fluences for gold targets. The required energy densities to ionize Au^{1+}, Au^{2+}, and Au^{3+} are labeled.

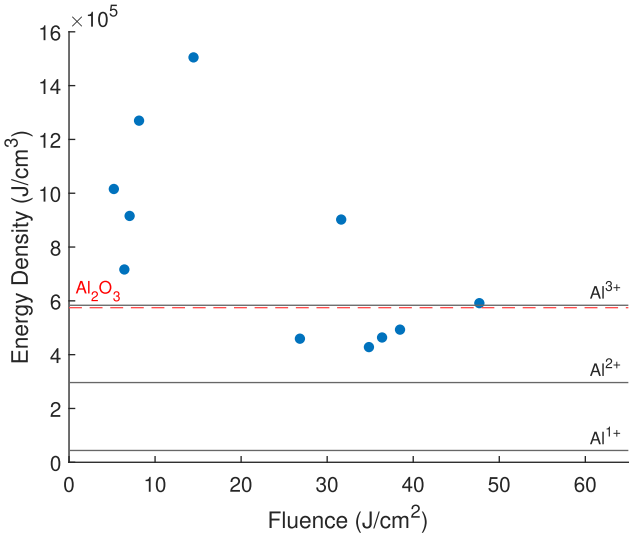

FIG. 5. The plasma energy density is determined from the experimental ablation volume as a function of experimental fluences for aluminum targets. The required energy densities to ionize Al^{1+}, Al^{2+}, Al^{3+} and to ablate Al_2O_3 (red) are labeled.

show the energy density as a function of fluence for gold, aluminum, and copper. This can be compared to the assumed ionization employed in the bleaching wave model as indicated in Figs. 8–10.

Figure 7 shows mass spectra for gold (a), aluminum (b), and copper (c) averaged over 100 single shots at fluences of 5.6, 5.2, and 3.2 J/cm^2, respectively, using EUV TOF. Peaks are identified for Au^{1+}, Au^{2+}, Al^{1+}, Al^{2+}, and Cu^{1+}, indicating that in the lower fluence range, there is an ionization level of up to 2+ for gold and aluminum and 1+ for copper. The data in Figs. 7(a) and 7(b) show that at lower fluences, the ablating plasma consists of 1+ and 2+ ions.

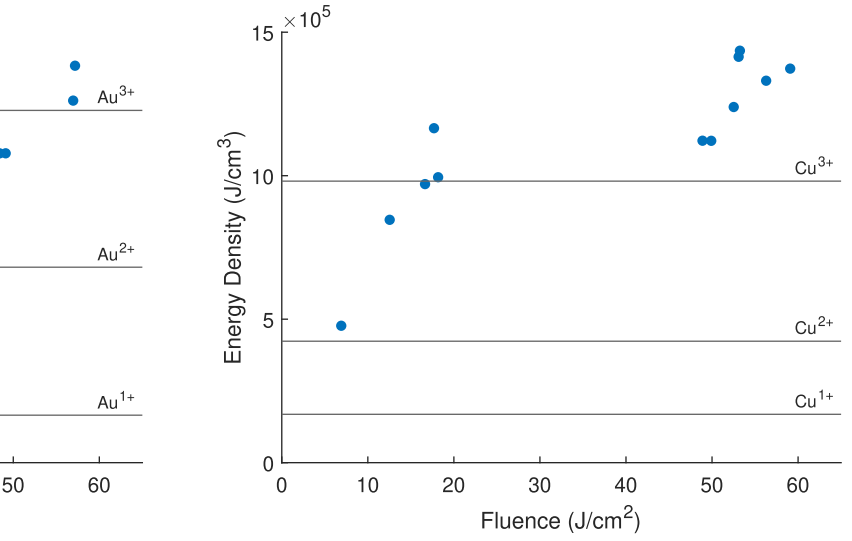

FIG. 6. The plasma energy density is determined from the experimental ablation volume as a function of experimental fluences for copper targets. The required energy densities to ionize Cu^{1+}, Cu^{2+}, and Cu^{3+} are labeled.

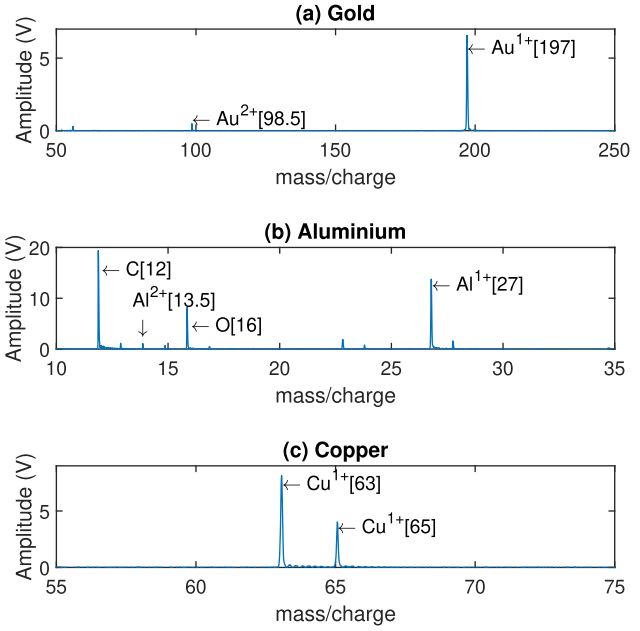

FIG. 7. Mass spectra averaged over 100 single shots for (a) gold, showing Au^{1+} at 197 and Au^{2+} at 98.5, with a fluence of 5.6 J/cm^2. (b) Aluminum, showing Al^{1+} at 27 and Al^{2+} at 13.5 with carbon at 12 and oxygen at 16, with a fluence of 5.2 J/cm^2. (c) Copper, showing two isotopes of Cu^{1+} at 63 and 65, with a fluence of 3.2 J/cm^2.

Figures 8–10 plot the resulting ablated crater depths as a function of the EUV laser fluence on each of the three target materials.

The experimental ablation depth results in Fig. 8 show an ablation depth agreement between low fluence experimental data and the model when Au^{1+} is the dominant ionization level. The mass

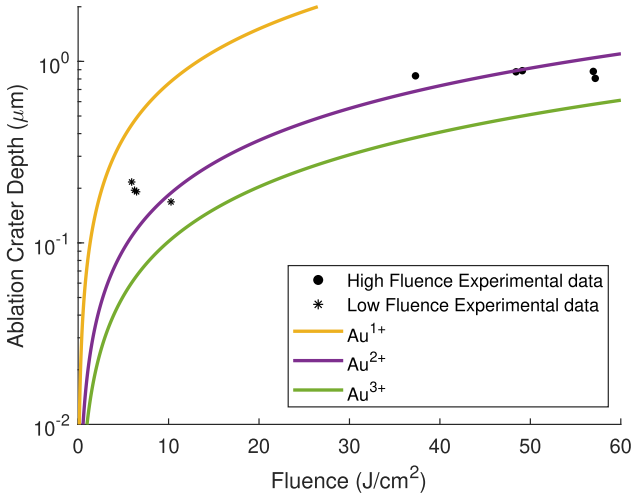

FIG. 8. Ablation depths as a function of fluence on target measured for a gold target. Ionization wave model predicted ablation depths are superimposed, assuming an ablated plasma ionized to Au^{1+} (yellow), Au^{2+} (purple), and Au^{3+} (green).

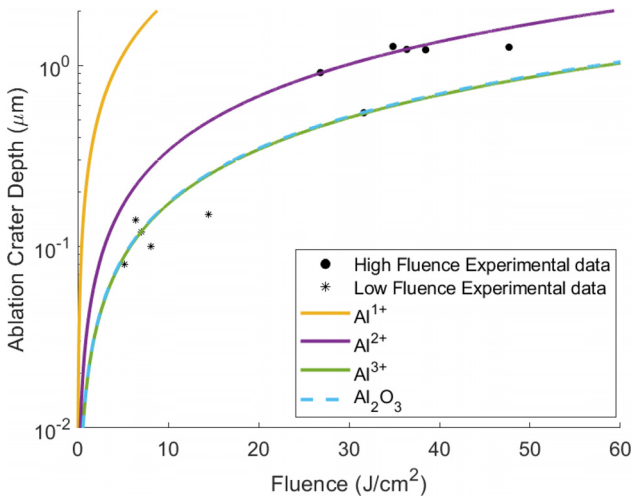

FIG. 9. Ablation depths as a function of fluence on target measured for an aluminum target. Ionization wave model predicted ablation depths are superimposed, assuming an ablated plasma ionized to Al^{1+} (yellow), Al^{2+} (purple), and Al^{3+} (green), and assuming Al_2O_3 ablates (blue dash coinciding closely with the Al^{3+} ionization.).

spectrometry results in Fig. 7(a) indicate that there is a smaller number of Au^{2+} ions produced at lower fluence, agreeing with the ablation crater profiles measured at those laser fluences. The model has predicted that as the laser fluence is increased, it is expected that the number of Au^{2+} ions also increases and becomes the dominant level of ionization. The high fluence ablation crater data match the model for higher ionization levels, indicating that at higher fluences, Au^{2+} becomes the dominant level of ionization. This is confirmed by comparing the energy density to E_{bleach}, where low fluence shots do not meet the required energy to ionize to Au^{2+}, but the higher fluence shots do meet these energy requirements (see Figs. 4–6). The experimental

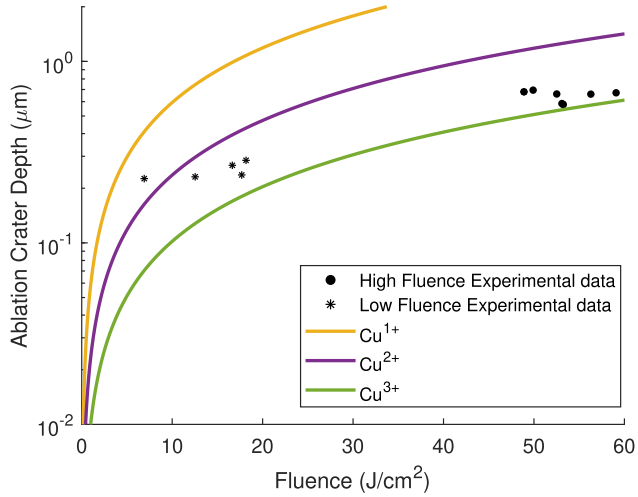

FIG. 10. Ablation depths as a function of fluence on target measured for a copper target. Ionization wave model predicted ablation depths are superimposed, assuming an ablated plasma ionized to Cu^{1+} (yellow), Cu^{2+} (purple), and Cu^{3+} (green).

ablation crater depth (see Fig. 8) shows a good correlation with the estimated depths for Au^{1+} at lower fluences ($<5\,J/cm^2$), and Au^{2+} and Au^{3+} at higher fluences ($>8\,J/cm^2$).

The EUV TOF mass spectrometry data in Fig. 7(b) show that the aluminum is ionized up to Al^{2+} for a fluence of $5.2\,J/cm^2$. The experimental data in Fig. 9 for fluences of $>20\,J/cm^2$ show that the plasma consists of a mixture of Al^{1+} and Al^{2+} ions. The depth of shots with fluences less than $20\,J/cm^2$ is slightly lower than what is estimated by the bleaching wave model caused by the aluminum oxide layer, which formed on the surface of the target. Figure 9 also shows the fluence required to ablate Al_2O_3 (blue dash). This has been calculated using the lattice enthalpy of Al_2O_3. The experimental data in Fig. 9 show that a thin layer of Al_2O_3 can reduce the depth of EUV ablation of aluminum as the energy to ablate Al_2O_3 exceeds the energy required to ionize and ablate pure aluminum to Al^+. This has a greater effect at lower fluences where there will be a higher ratio of Al_2O_3 to Al in the amount of material ablated.

The copper ablation results in Fig. 10 show that as the fluence increases the experimental ablation depths are best fitted with an assumed higher ion charge. Experimental results below $5\,J/cm^2$ are most similar to the ionization wave for Cu^{1+}, which is confirmed in Fig. 7(c) at a fluence of $3.2\,J/cm^2$. At slightly higher fluences, from 9 to $15\,J/cm^2$, the depths imply a dominant ion charge closer to Cu^{2+}, and for fluences above $30\,J/cm^2$, the experimental results imply dominant ionization closer to Cu^{3+} for the wave model. This is in agreement with the energy density, with fluences $>10\,J/cm^2$ ionized up to Cu^{2+} and $>20\,J/cm^2$ ionized up to Cu^{3+}.

The investigation presents experimental results into the ablation of metal targets of gold, aluminum, and copper using an EUV capillary discharge laser at a wavelength of 46.9 nm. Data were recorded using two laser systems, a high fluence system (Fig. 1) using a high energy EUV capillary discharge laser and large reflective optics to ablate the metal targets. The low fluence system (Fig. 2) has a lower energy EUV capillary discharge laser system focused using a Fresnel zone plate, the mass-to-charge ratio of the ions produced in the ablation plasma is

measured using a time-of-flight mass spectrometer. The low fluence data show that the dominant level of ionization of the plasma and the ablation crater depth is in agreement with the traveling wave model developed by Tallents *et al.*[14] The higher fluence data show that with increasing fluence, the trend of the ablation crater depth follows that estimated by the model, thus, an estimation of the dominant level of ionization within the plasma can be made. The degree of ionization used in the model fits to the ablation depth measurements and is consistent with the energy density of ablated plasma, assuming all the laser energy is absorbed in the ablated volume. This work has confirmed the relationship between the laser fluence, crater depth, and plasma composition, enabling future studies into alternative target materials and fluence ranges.

ACKNOWLEDGMENTS

We acknowledge the EPSRC Centre for Doctoral Training in the Science and Technology of Fusion Energy (EP/L01663X/1), especially the internationalization funding, and the NSF PFI-TT for enhancing the mass production of advanced integrated circuits (2141227).

AUTHOR DECLARATIONS

Conflict of Interest

The authors have no conflicts to disclose.

Author Contributions

S. A. Wilson: Conceptualization (lead); Data curation (lead); Formal analysis (lead); Funding acquisition (supporting); Investigation (lead); Methodology (lead); Project administration (lead); Resources (lead); Software (lead); Validation (lead); Visualization (equal); Writing – original draft (lead); Writing – review & editing (equal). **L. A. Rush:** Data curation (supporting); Formal analysis (supporting); Investigation (supporting); Methodology (supporting); Validation (supporting); Visualization (supporting); Writing – original draft (supporting). **E. Solis Meza:** Data curation (supporting); Formal analysis (supporting); Validation (supporting). **J. A. Lolley:** Data curation (supporting); Investigation (supporting). **J. J. Rocca:** Supervision (supporting). **C. S. Menoni:** Supervision (supporting); Visualization (supporting); Writing – review & editing (equal). **G. J. Tallents:** Conceptualization (supporting); Funding acquisition (lead); Supervision (lead).

DATA AVAILABILITY

The data that support the findings of this study are available from the corresponding author upon reasonable request.

REFERENCES

[1]F. Frassetto, S. Bonora, P. Villoresi, L. Poletto, E. Springate, C. A. Froud, I. C. E. Turcu, A. J. Langley, D. S. Wolff, J. L. Collier, S. S. Dhesi, and A. Cavalleri, "Design and characterization of the XUV monochromator for ultrashort pulses at the ARTEMIS facility," Proc. SPIE **7077**, 707713 (2008).
[2]G. Tallents, E. Wagenaars, and G. Pert, "Optical lithography: Lithography at EUV wavelengths," Nat. Photonics **4**, 809–811 (2010).
[3]H. Bravo, B. T. Szapiro, P. W. Wachulak, M. C. Marconi, W. Chao, E. H. Anderson, C. S. Menoni, and J. J. Rocca, "Demonstration of nanomachining with focused extreme ultraviolet laser beams," IEEE J. Sel. Top. Quantum Electron. **18**, 443–448 (2012).
[4]A. K. Rossall and G. J. Tallents, "Generation of warm dense matter using an argon based capillary discharge laser," High Energy Density Phys. **15**, 67–70 (2015).
[5]T. Tomie, "Tin laser-produced plasma as the light source for extreme ultraviolet lithography high-volume manufacturing: History, ideal plasma, present status, and prospects," J. Micro/Nanolithogr., MEMS, MOEMS **11**, 21101–21109 (2012).
[6]I. Kuznetsov, J. Filevich, F. Dong, M. Woolston, W. Chao, E. H. Anderson, E. R. Bernstein, D. C. Crick, J. J. Rocca, and C. S. Menoni, "Three-dimensional nanoscale molecular imaging by extreme ultraviolet laser ablation mass spectrometry," Nat. Commun. **6**, 6944 (2015).
[7]T. Green, I. Kuznetsov, D. Willingham, B. E. Naes, G. C. Eiden, Z. Zhu, W. Chao, J. J. Rocca, C. S. Menoni, and A. M. Duffin, "Characterization of extreme ultraviolet laser ablation mass spectrometry for actinide trace analysis and nanoscale isotopic imaging," J. Anal. At. Spectrom. **32**, 1092–1100 (2017).
[8]L. A. Rush, J. B. Cliff, D. D. Reilly, A. M. Duffin, and C. S. Menoni, "Isotopic heterogeneity imaged in a uranium fuel pellet with extreme ultraviolet laser ablation and ionization time-of-flight mass spectrometry," Anal. Chem. **93**, 1016–1024 (2021).
[9]N. Tanaka, M. Masuda, R. Deguchi, M. Murakami, A. Sunahara, S. Fujioka, A. Yogo, and H. Nishimura, "Characterization of material ablation driven by laser generated intense extreme ultraviolet light," Appl. Phys. Lett. **107**, 114101 (2015).
[10]I. A. Artyukov, B. R. Benware, A. V. Vinogradov, Y. S. Kas'yanov, V. V. Kondratenko, C. Macchietto, A. Ozols, J. J. Rocca, and J. Chilla, "Focusing the beam of a compact, repetitively pulsed x-ray laser to study the interaction of radiation with metallic targets and x-ray reflectrometry," Quantum Electron. **30**, 328–332 (2000).
[11]V. Aslanyan, I. Kuznetsov, H. Bravo, M. R. Woolston, A. K. Rossall, C. S. Menoni, J. J. Rocca, and G. J. Tallents, "Ablation and transmission of thin solid targets irradiated by intense extreme ultraviolet laser radiation," APL Photonics **1**, 066101 (2016).
[12]J. J. Rocca, V. Shlyaptsev, F. G. Tomasel, O. D. Cortzar, D. Hartshorn, and J. L. A. Chilla, "Demonstration of a discharge pumped table-top soft-x-ray laser," Phys. Rev. Lett. **73**, 2192–2195 (1994).
[13]M. Berrill, F. Brizuela, B. Langdon, H. Bravo, C. S. Menoni, and J. J. Rocca, "Warm photoionized plasmas created by soft-x-ray laser irradiation of solid targets," J. Opt. Soc. Am. B **25**, B32–B38 (2008).
[14]G. J. Tallents, D. S. Whittaker, L. A. Wilson, and E. Wagenaars, "Heating of high energy density plasmas using EUV and x-ray lasers," Proc. SPIE **8140**, 81400F (2011).
[15]J. J. Rocca, "Table-top soft x-ray lasers," Rev. Sci. Instrum. **70**, 3799–3827 (1999).
[16]S. Heinbuch, M. Grisham, D. Martz, and J. J. Rocca, "Demonstration of a desktop size high repetition rate soft x-ray laser," Opt. Express **13**, 4050 (2005).
[17]S. A. Wilson, "A study of extreme ultraviolet capillary discharge lasers and the ablation of solid targets," Ph.D. thesis (The University of York, 2018).
[18]I. Kuznetsov, "Extreme ultraviolet laser ablation mass spectrometer for molecular imaging at the nanoscale," Ph.D. thesis (Colorado State University, 2018).